Acceleration of Tissue Plasminogen Activator-Mediated Thrombolysis by Magnetically Powered Nanomotors

Rui Cheng,[†,¶] Weijie Huang,[‡,¶] Lijie Huang,[§,⊥] Bo Yang,[∥] Leidong Mao,[†,*] Kunlin Jin,[§] Qichuan ZhuGe,[⊥] and Yiping Zhao[‡,*]

[†]College of Engineering and [‡]Department of Physics and Astronomy, Nanoscale Science and Engineering Center, University of Georgia, Athens, Georgia 30602, United States, [§]Department of Pharmacology and Neuroscience, Institute for Alzheimer's Disease and Aging Research, University of North Texas Health Science Center, Fort Worth, Texas 76107, United States, [⊥]Zhejiang Provincial Key Laboratory of Aging and Neurological Disorder Research, The First Affiliated Hospital of Wenzhou Medical University, Wenzhou, Zhejiang 325000, China, and [∥]Department of Mechanical and Aerospace Engineering, University of Texas, Arlington, Texas 76019, United States. [¶]These authors contributed equally.

ABSTRACT Dose control and effectiveness promotion of tissue plasminogen activator (t-PA) for thrombolysis are vitally important to alleviate serious side effects such as hemorrhage in stroke treatments. In order to increase the effectiveness and reduce the risk of stroke treatment, we use rotating magnetic nanomotors to enhance the mass transport of t-PA molecules at the blood clot interface for local ischemic stroke therapy. The *in vitro* experiments demonstrate that, when combined with magnetically activated nanomotors, the thrombolysis speed of low-concentration t-PA (50 μg mL^{-1}) can be enhanced up to 2-fold, to the maximum lysis speed at high t-PA concentration. Based on the convection enhanced transport theory due to rotating magnetic nanomotors, a theoretical model is proposed and predicts the experimental results reasonably well. The validity and efficiency of this enhanced treatment has been demonstrated in a rat embolic model.

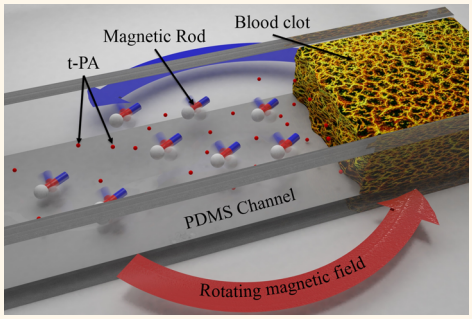

KEYWORDS: nanomotor · magnetic nanorods · stroke · acceleration of thrombolysis · enhanced mass transport

Stroke is the second leading cause of death and the leading cause of disability among adults worldwide according to the World Health Organization (WHO). Despite testing over 70 agents in clinical trials, only one of them has been approved by the Food and Drug Administration (FDA) for the treatment of ischemic stroke. This drug, recombinant tissue plasminogen activator (rt-PA or t-PA), can activate plasminogen to plasmin, which then binds to fibrin and breaks up the blood clot in cerebral blood vessels. While the t-PA treatment of blood clot is considered to be safe, side effects occurring in some patients have raised major concerns about the safety and the efficacy of t-PA treatment. Current acute therapy of stroke requires infusion of t-PA drug through a catheter placed within the blocked vessel. It has been reported that, in about 6−7% cases, the usage of t-PA can cause symptomatic intracranial hemorrhages (SIH) because t-PA is free to diffuse throughout the body.[1] SIH may lead to death if it is left unattended, and in about half of the cases, the t-PA fails to lyse the clot and recanalize the middle cerebral artery.[2] As a result, t-PA treatment is rarely suitable for ischemic stroke patients and is used only in about 1−2% of them.[3] Clearly, in order to improve this therapy, new strategies with better safety and improved effectiveness are needed.

So far, dose control and effectiveness promotion of drugs are the main approaches to reduce the risks of SIH associated with stroke treatment. A few promising approaches have been developed recently. In particular, nanocarrier drug delivery is the most widely used method because of its advantages in accurate dose control by nanosynthesis and precise targeting by dynamic delivery system.[4] Specifically for thrombolytic medications, different nanocarrier fabrication strategies and targeting methods have been proposed

* Address correspondence to mao@uga.edu, zhaoy@physast.uga.edu.

Received for review February 4, 2014 and accepted July 9, 2014.

Published online July 09, 2014
10.1021/nn5029955

and tested. For example, thrombolytic drugs have been incorporated with magnetic nanoparticles and delivered to the clot site with an external magnetic field. The drug delivered by magnetic nanoparticles could interact with the fibrins of the blood clot locally. In most cases, Fe_3O_4 or γ-Fe_2O_3 nanoparticles are preferred due to their strong magnetic properties and good biocompatibility.[5,6] Some magnetic nanocarriers are fabricated by encapsulating both magnetite and t-PA using a biodegradable matrix, such as polyethylene glycol−polylactic acid copolymer.[7] Some are core−shell nanoparticles with a superparamagnetic iron oxide core and a functionalized shell binding to drugs such as t-PA.[8] Compared to normal treatments, the nanocarrier method requires a much smaller amount of drug because the drug is greatly localized. As a result, the drug's side effect is reduced. In addition, nonmagnetic nanoparticles coated by both thrombolytic enzymes and fibrin-specific ligands not only can deliver the drug to the fibrin but also can cover the clotting surface to form a thrombin-inhibiting coating that could theoretically reduce further thrombus formation as the particles continue to bind on the thrombin.[9] Recently, another passively targeting method named "shear-active nanotheraputics" has been developed by taking advantage of the distortion of the bloodstream caused by the clot itself.[10] The drug carrier is a biocompatible and biodegradable poly(lactic-*co*-glycolic) microaggregate composed of t-PA-coated nanoparticles. Such microaggregates can hold the nanoparticles together in the normal bloodstream, while under high shear rate blood flow, they break and release nanoparticles due to the presence of the clot. The amount of drug released can be controlled by the number of nanoparticles. However, for the methods mentioned above, highly specialized nanocarriers need to be fabricated to load specific drugs, and the drug's effectiveness may be limited by the loading rate of nanocarriers. Furthermore, for the t-PA loaded on nanocarriers, its effectiveness could be compromised due to the dependence of t-PA's activity on conformational-induced activation during the fibrin binding process.[11]

Looking at the nanocarrier-based stroke treatment from a new angle, the question we are asking is once the t-PA drug and nanocarriers are delivered near the blood clot, can we further increase the therapeutic effectiveness through mechanical motions of nanocarriers? In this paper, the answer is sought through the usage of magnetically activated nanomotors to mechanically agitate the t-PA drug and the study of its therapeutic effect. We demonstrate in an *in vitro* system that the thrombolytic speed associated with this proposed treatment can be almost doubled and reach its maximum efficiency without increasing the t-PA dose. The underlying reason for this enhancement is investigated through the convection enhanced diffusion/mass transport of t-PA molecules toward the fibrin surfaces. The theoretical predications match reasonably well to the *in vitro* experimental results. In the end, this treatment results in improved clot removal as demonstrated in a rat embolic model.

RESULTS AND DISCUSSION

According to the guidelines for the management of patients with acute ischemic stroke published by the American Heart Association Stroke Council (2007),[12] the dosing regimen of intravenous t-PA treatment is 0.9 mg/kg (maximum of 90 mg per treatment).[13] The ratio of blood volume to body weight ranges from 62 to 86 mL/kg, corresponding to population groups which vary from 25% underweight and 16% overweight.[14] Thus, the average t-PA concentration in blood ranges from 10.5 to 14.5 μg/mL during the intravenous administration, which is consistent with the statistic results.[15,16] According to the recanalization time,[17] the average size, and the configuration of blood clots in blood vessels,[18] the clot lysis process under usual clinically administrative t-PA concentration is a diffusion-limited process or a mass-transport-limited process depending closely on the t-PA bulk concentration.[19−24] This is further confirmed by the *in vitro* experiments carried out in an 8-channel polydimethylsiloxane (PDMS) fluidic plate mounted on top of a light pad and between two pairs of solenoids (for detailed experimental setup, see Supporting Information 1.1). As shown in Figures S1a and S2, on the right ends of the PDMS channels, uniform and equal-length clots are fabricated. Dye solutions mixed with different concentrations of t-PA are injected to the left of the clot sections and sealed by mineral oil from the left end to prevent solution evaporation during the experiments. The dye concentration in all channels is fixed at 0.5 mM, while the t-PA concentration varies from 12.5 to 1600 μg mL^{-1}. It is observed that the dye/clot interface of all channels advances to the right, that is, to the clot section. The boundary of dye and clot interface was defined as the location of maximum dye concentration gradient. Quantitative data on the clot lysis speed can be obtained through movie and image analyses based on dye concentration calibration and software developed in our lab. The experiment results are summarized in Figure S5. At low $C_{t\text{-}PA}$ ($\leq$60 μg mL^{-1}), the clot lysis speed v_T increases almost linearly with $C_{t\text{-}PA}$, and when $C_{t\text{-}PA} \geq 200$ μg mL^{-1}, v_T reaches a maximum value of 55 μm min^{-1}. Thus, at $C_{t\text{-}PA} \leq 60$ μg mL^{-1} (clinically administrative t-PA concentration), the thrombolysis process is a diffusion-limited process. Therefore, in order to enhance the thrombolysis but keep the t-PA concentration low, it is important to improve the mass transport process during thrombolysis, and we believe that such a mass transport enhancement can be achieved by rotating nanorods.

As schematically illustrated in Figure 1, the proposed strategy is to mix t-PA solution with magnetic nanorod suspension and to rotate the nanorods remotely by a rotating magnetic field. We expect that the rotating nanorods can enhance the t-PA thrombolysis speed through enhanced mass transport. The magnetic rods used in this proof-of-principle study are nickel (Ni) nanorods fabricated by oblique angle deposition (OAD) method and suspended in polyvinylpyrrolidone (PVP), as shown in Figure 2.[25] To test the effect of rotating nanorods, four different solutions were injected to the PDMS channels (see Supporting Information 1): dye solutions, denoted as "*D*"; t-PA mixed with dye solution, denoted as "*T*"; nanorod−dye mixture solution, denoted as "*R*"; and dye, t-PA, and nanorod mixture solution, denoted as "*R*+*T*", as shown in Figure 3b. The $C_{t\text{-}PA}$ in "*T*" and "*R*+*T*" channels is designed to be the same, 50 μg mL^{-1}. In both "*R*" and "*R*+*T*" channels the nanorod concentration C_R has been changed systematically from 1 to 7 mg mL^{-1}. Figure 3b also shows the representative snapshots of the moving t-PA and clot interface at different time for C_R = 7 mg mL^{-1}. At the t-PA/clot interfaces, all interface fronts in the "*R*" and "*D*" channels remain almost fixed while the interfaces at all the "*T*" and "*R*+*T*" channels advance to the right. It is observed that the interfaces of the "*R*+*T*" channels move faster than those of the "*T*" channels (see supporting movie 1). Figure 3c plots the one-dimensional grayscale distribution of dye along four representative channels at four different times, shown in Figure 3c. The lysis speed in each channel was assumed to be proportional to the boundary moving speed. For both the "*D*" and "*R*" channels, the grayscale profiles shows diffusion like behavior. The boundaries move slightly, but the profiles become more broadened. Using the dye concentration calibration curve with respect to the grayscale, and taking the first derivation of the profile, one can obtain how the dye moves into the clot (see Supporting Information 1.2 for details). From the width *versus* time plot in the "*D*" channel, we can extract the diffusion coefficient of dye to be 27.7 ± 0.6 μm^2 s^{-1}. For the "*R*" channel, the obtained diffusion coefficient is determined to be 42.4 ± 0.6 μm^2 s^{-1}, which is slightly larger than that in the "*D*" channel. This is an indication of rotating nanorod enhanced molecular diffusion. For both "*T*" and "*R*+*T*" channels, the grayscale profile maintains its overall shape but advances to the right quickly. Clearly, the "*R*+*T*" profile advances faster than the "*T*" profile. In fact, for C_R = 7 mg/mL, the average thrombolysis speed v_T for "*T*" channel is 24.8 ± 0.5 μm min^{-1}, and the average enhanced thrombolysis speed v_{R+T} in the "*R*+*T*" channel is 68 ± 36 μm min^{-1}, as shown in Figure 3d. This speed is close to the maximum lysis speed at very high t-PA concentration ($C_{t\text{-}PA} \geq$ 100 μg mL^{-1}). By varying the nanorod concentration, C_R, and keeping all the other conditions constant, one observes that the thrombolysis speed v_{R+T} increases monotonically as a function of rod concentration C_R. Figure 3d plots v_T and v_{R+T} *versus* C_R. One can see that, at different C_R, v_T fluctuates within 29 ± 6 μm min^{-1} while v_{R+T} increases monotonically with C_R. This enhanced thrombolysis rate v_{R+T} could be due to two possible reasons: a mechanically ruptured clot network or the enhanced mass transport of t-PA and lysis

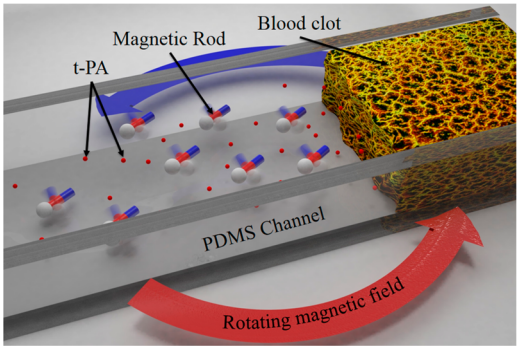

Figure 1. Schematic view of nanomotor enhanced thrombolysis in fluidic channels. The magnetized nickel rods are dispersed in t-PA solution and activated by a rotational magnetic field at the vicinity of a clot in a PDMS channel. The mass transport of t-PA molecules is directly accelerated by the hydrodynamic flows induced by rotating nanorods.

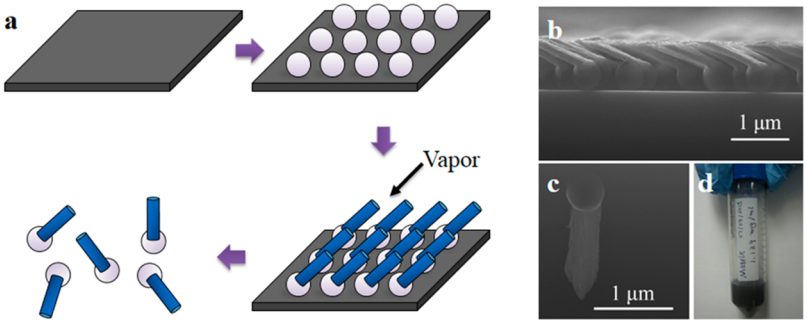

Figure 2. Nickel rod fabrication process using OAD and convective self-assembly methods. (a) Schematic process of fabrication indicated in clockwise direction: self-assembled monolayer of polystyrene beads on a cleaned silicon wafer; uniform nickel rods grown on beads using OAD method; rods washed into suspension of PVP. (b) Side view of nanorods on silicon substrate. (c) Single nanorod with a polystyrene bead. (d) Rods suspended in PVP (MW = 40K Da) solution, forming a matrix of known concentration.

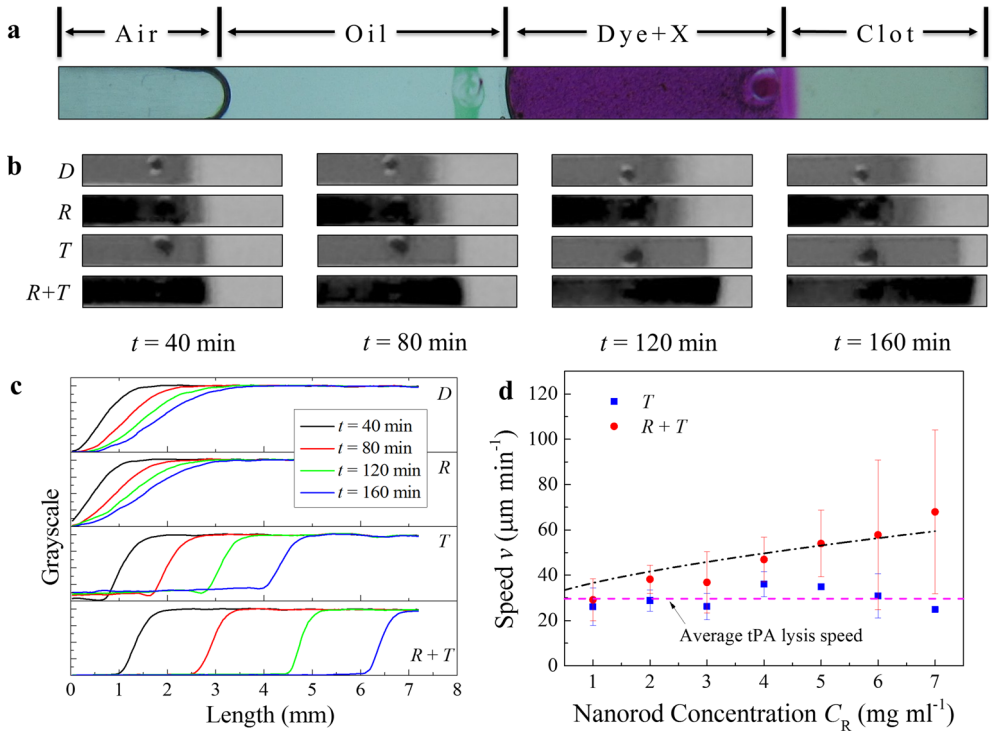

Figure 3. Results of *in vitro* experiments. (a) Representative PDMS channel structure, where "X" represents different mixtures. (b) Video clips of green channel images at the liquid/clot interface in "*D*", "*R*", "*T*", and "*R*+*T*" channels (from top to bottom), at different thrombolysis times *t* = 40, 80, 120, and 160 min (from left to right), respectively. (c) Plot of grayscale *versus* PDMS channel location in (b). (d) Clot boundary moving speed v_T and v_{R+T} *versus* nanorod concentration C_R. The blue solid square represents v_T, and the red solid circle represents v_{R+T}. The pink dashed line is a guide for eyes, and the black dash-point curve is a fitting curve based on the proposed theoretical model.

products caused by nanorod rotation. Both our experimental observation and theoretical simulation based on the force/torque induced by the nanorods and mechanical properties of fibrins suggest that the mechanically induced rupture could not be the major reason for the enhanced thrombolysis speed (for details, see Supporting Information 2.4). Since at $C_{t\text{-}PA}$ = 50 μg/mL, the thrombolysis process is mass-transport-limited, while the rotation of the nanorods could induce local convection flows to enhanced reactant diffusion. It is very likely that the observed enhanced thrombolysis speed is caused by the enhanced mass transport as illustrated in Figure 4a.

The detailed t-PA clot lysis process is shown in Figure 4b. In plasma with absence of fibrin, t-PA activates the plasminogen into plasmin at a very low efficiency and the plasmin cannot survive in plasma due to its strong affinity for the plasmin inhibitor. However, the lysine sites on fibrin attract both t-PA and plasminogen molecules and assemble them on the fibrin surface where the plasminogen can be activated by t-PA at a high efficiency. Furthermore, the activated plasmin can be protected from the plasmin inhibitor in plasma.[26−30] Eventually, the fibrin is cleaved by plasmin into a soluble product. This complicated molecular process can be treated as a three-step event (see Supporting Information 2.1): (1) t-PA molecules (T) diffuse to the fibrin surface and bind onto fibrin lysine sites (S) to form t-PA−lysine complex (ST); (2) t-PA−lysine complex (ST) activates plasminogen into plasmin which cleaves fibrin into soluble product (P); (3) product (P) desorbs from the fibrin surface and exposes new lysine sites. Thus, the process can be described as

$$S + T \xrightarrow{k_T} ST(SP) \xrightarrow{k_P} S + P$$

with t-PA absorption rate k_T, product desorption rate k_P, and a fast transition reaction ST → SP. When the reaction reaches a steady state, the thrombolysis speed is proportional to the reaction rate of desorbed product molecule *P*, with $(dN_P)/(dt) = (k_T k_P)/(k_T + k_P)$, where N_P is the number of product molecule P. Assuming that the transport-facilitated t-PA binding is the rate-limiting step at $C_{t\text{-}PA}$ = 50 μg/mL, that is, $k_P \gg k_T$, then $(dN_P)/(dt) = k_T$. If each molecule P produced in the thrombolysis frees a volume V_P from the solid clot, then the thrombolysis speed observed in the channel can be expressed as $v_{R+T} = V_P k_T/(A_c(1 - \Phi))$, where A_c is the cross-section area of the PDMS channel, Φ is the porosity of the clot, and both can be assumed to be a constant. According to the von Smoluchowski's equation, the reaction rate k_T for a diffusion-limited reaction is given by $k_T = 4\pi D_{t\text{-}PA}(R_{t\text{-}PA} + R_{site})C_{t\text{-}PA}$.[31] Here $D_{t\text{-}PA}$ is the effective diffusivity of t-PA enhanced by rotating nanorods, and $R_{t\text{-}PA}$ and R_{site} are the radii of t-PA

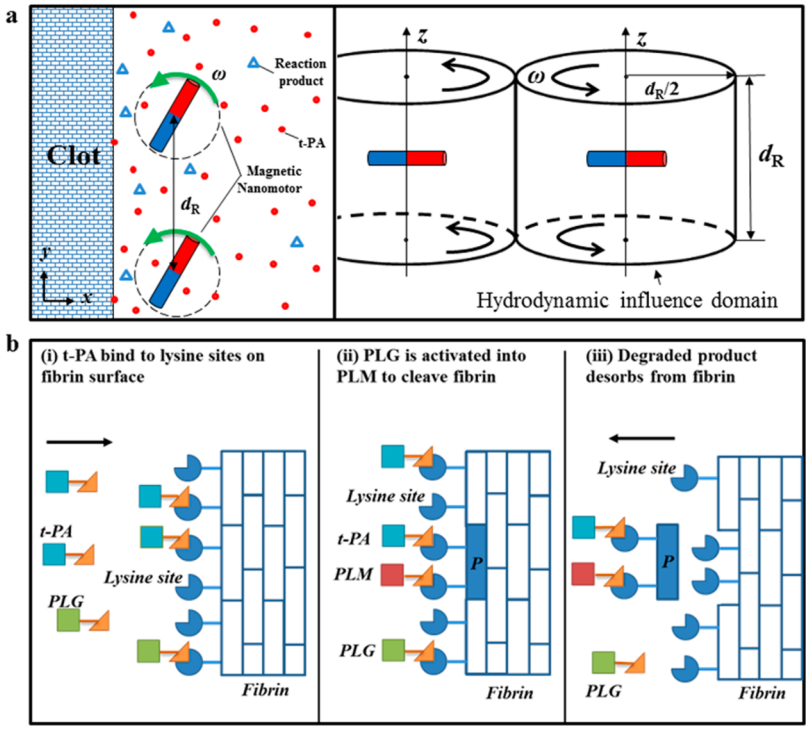

Figure 4. Schematic illustration of t-PA-mediated thrombolysis enhanced by the nanomotors at the liquid/clot interface. (a) Hydrodynamic induced mobility: when a nanorod in solution is driven by a rotational magnetic field, it will induce a creepy Stokes' flow. The flow has a cylindrical hydrodynamic influence. The overall effect on the transport of t-PA and lysis molecules can be estimated as hydrodynamic agitation and provides an additional mobility besides thermal diffusion. (b) Simplified schemes of t-PA-mediated thrombolytic reaction on the clot surface: (i) t-PA and plasminogen (PLG) molecules diffuse to the clot surface and bind to lysine sites. (ii) PLG molecules on the fibrin surface are activated into plasmin (PLM) by the neighboring t-PA molecules. PLM molecules start to cleave the local fibrin fiber into soluble products (P). (iii) Lysis molecules P leave the fibrin surface and expose new lysine sites.

molecules and lysine sites. The hydrodynamic enhanced diffusivity $D_{t\text{-}PA}$ can be expressed as $D_{t\text{-}PA} = D^T_{t\text{-}PA} + D^C_{t\text{-}PA}$, where $D^T_{t\text{-}PA}$ is the thermally induced diffusion coefficient given by Einstein's equation $D^T_{t\text{-}PA} = (k_BT)/(6\pi\eta R_{t\text{-}PA})$ and $D^C_{t\text{-}PA}$ is convectional flow enhanced diffusion by rotating rods. The detailed expression for $D^C_{t\text{-}PA}$ is determined by the Peclet number Pe, $Pe = (\bar{u}d_R)/(D^T_{t\text{-}PA})$, where $d_R = C_{NR}^{-1/3}$ is the size of each cellular flow induced by a rotating rod, C_{NR} is the number concentration of the rods, and $\bar{u}$ is the average velocity of the flow field induced by the nanorods. Assuming that nanorods are uniformly distributed in the solution and neglecting the nanorod interaction, an individual rotating nanorod can be modeled as a torque and induce a Stokes' creeping flow at low Reynolds number, $\bar{u}$ can be expressed as $\bar{u} = (|\vec{M}|(\chi C_R)^{2/3})/4\eta \times \ln(1 + \sqrt{2})$, where η is the fluid viscosity, $|\vec{M}|$ is a singular point torque by a rotating nanorod and χ is a unit convertor so that $C_{NR} = \chi_{CR}$ (for details, see Supporting Information 2.2). The estimated Pe varies from 1.6 to 3.1 when C_R changes from 1 to 7 mg/mL in the experiments. According to the convection enhanced diffusion theory, when the Peclet number Pe is small (Pe < 3),[32] the flow scaling law is valid for rigid boundary conditions and the enhanced diffusivity can be estimated as[33,34] $D_{t\text{-}PA} = D^T_{t\text{-}PA}(1 + a\mathrm{Pe}^2)$, where a is a constant (=$2/3\pi^2$ in a spatially periodic hydrodynamic flow[34]). Since $\mathrm{Pe} \propto C_R^{1/3}$, the clot boundary moving speed can be estimate as

$$v_{R+T} = v_T + \alpha C_R^{2/3} \quad (1)$$

where

$$v_T = \frac{4\pi(R_{t\text{-}PA\times} + R_{site})V_P}{A_c(1 - \Phi)} C_{t\text{-}PA} D^T_{t\text{-}PA}$$

is the t-PA-mediated thrombolysis rate without nanorods in the channel and is proportional to the concentration and thermal diffusivity of t-PA, and

$$\alpha = C_{t\text{-}PA}\frac{4\pi(R_{t\text{-}PA} + R_{site})V_P}{A_c(1 - \Phi)} \frac{0.0486a|\vec{M}|^2\chi^{2/3}}{\eta^2 D^T_{t\text{-}PA}}$$

is a parameter related to the enhancement of thrombolysis. Equation 1 can fit the experimental data in Figure 3d very well, as shown by the dash-dotted curve, and we obtain $v_T = 28 \pm 2\ \mu\mathrm{m\ min^{-1}}$ and $\alpha = (9 \pm 2) \times 10^{-4}\ \mathrm{mL\ mg^{-2/3}\ min^{-1}}$. In fact, the α value can also be estimated theoretically according to the known parameters (see Supporting Information 2.2), and we obtain $\alpha = 1.59 \times 10^{-4}\ \mathrm{mL\ mg^{-2/3}\ min^{-1}}$, which is on the same order of magnitude of the experimental value. The match between the theoretical

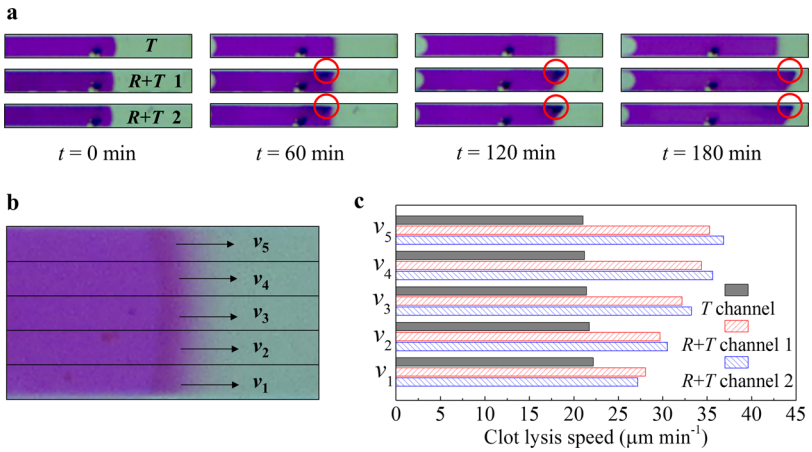

Figure 5. Locally enhanced thrombolysis through concentrating nanorods. (a) Video clips of dye solution/clot interface evolution in one "*T*" and two "*R*+*T*" channels with C_R = 1 mg mL^{-1} with a nail presented in the magnetic field. Red circles indicate locations of the concentrated magnetic nanorods. (b) Each channel is horizontally divided into 5 subchannels of equal width, and the moving speed of the liquid/clot interface in each subchannel is labeled as v_1, v_2, v_3, v_4, and v_5, from bottom to top. (c) Local clot lysis rate of three channels. Due to the conjugation of the nanorod at the top-right corner in two "*R*+*T*" channels, the lysis rate is increased from v_1 to v_5. The enhanced thrombolysis factor β can be up to 1.75, which is comparable to v_{R+T} at C_R = 5 mg mL^{-1} shown in Figure 3d.

prediction and experimental data further validates the mechanism of enhanced mass transport for thrombolysis.

However, we also notice that in Figure 3d the error bar of v_{R+T} is increasing by C_R. This is mainly due to the clustering effect of magnetic nanorods under rotating field (see Supporting Information 2.3). We observe that, without applying the magnetic field, the rods of both low and high concentration suspended in the solution are uniformly distributed; when a uniform static magnetic field is applied, the rods will form chain-like clusters due to the magnetic dipole−dipole interaction.[35] When the magnetic field starts to rotate, such chain-like clusters will either remain rotating as "big rods" or break into smaller rotating rod clusters, and the standard deviation of the cluster size distribution δn increases monotonically with C_R. If each cluster can be treated as a rigid particle, according to a modified eq 1, we can predict that the error bar for v_{R+T} is proportional to δn (see Supporting Information 2.3).

Our model also indicates that the rotation of the nanorods near the clot/solution interface in fact should be more effective compared to locations far away from the interface. This means that, if the local concentration of the nanorods at the fibrin interface is high, one can obtain similar lysis speed as for a high global concentration; that is, if the nanorods can be concentrated at the clot/solution interface, one can achieve a high lysis rate at a low global concentration. We have designed an experiment to demonstrate this effect. The *in vitro* experiment at C_R = 1 mg mL^{-1} was repeated with all the other experimental conditions fixed except adding an iron nail at the right end of the PDMS device, close to the clot segments. Due to the higher magnetic permeability of the nail, there is a local field maximum of magnetic field that attracts nanorods toward the clot interface and makes them stay at the clot/solution boundary during the experiment. Thus, the local concentration of rods at the clot/solution interface is greatly increased. As shown in Figure 5a, the rods are uniformly distributed in the "*R*+*T*" channels at t = 0 min. When the magnetic field is on, the rods are concentrated at the clot boundaries and form a taper shape. To evaluate the location-dependent thrombolysis rate, each channel in Figure 5a is horizontally divided into 5 subchannels of equal width, as shown in Figure 5b of the "*T*" channel. The moving speeds of liquid/clot interface at different subchannels, from bottom to top, are estimated as v_1, v_2, v_3, v_4, and v_5. According to the results shown in Figure 5c, the thrombolysis rates v_T in subchannels of "*T*" are very uniform with an average value of 22.2 ± 0.1 μm min^{-1}. Remarkably, the thrombolysis rates v_{R+T} in subchannels of "*R*+*T*" increase from v_1 to v_5 due to the gradual accumulation of nanorods toward the top-right corner at the boundary. The maximum thrombolysis rate v_{R+T} at different locations in "*R*+*T*" channels is up to 36.8 ± 0.4 μm min^{-1}. Thus, the enhanced thrombolysis factor $\beta = v_{R+T}/v_T$ can be up to 1.66. However, for C_R = 1 mg mL^{-1} with uniform nanorod distribution shown in Figure 3d, v_{R+T} = 29 ± 9 μm min^{-1} while v_T = 26 ± 8 μm min^{-1}, and β = 1.1. Thus, for the same C_R, the thrombolysis enhancement by rods concentrated at the clot/solution interface (see movie 2, C_R = 1 mg mL^{-1}) is significantly larger than that when the rods are distributed uniformly and activated over the whole solution (see movie 3, C_R = 1 mg mL^{-1}). In fact, as shown in Figure 3d, the β of locally concentrated rods with C_R = 1 mg mL^{-1} is comparable to that of C_R = 5 mg mL^{-1} with uniform nanorod distribution. The results demonstrate that by concentrating magnetic nanorods at the clot/liquid interface, even with a low

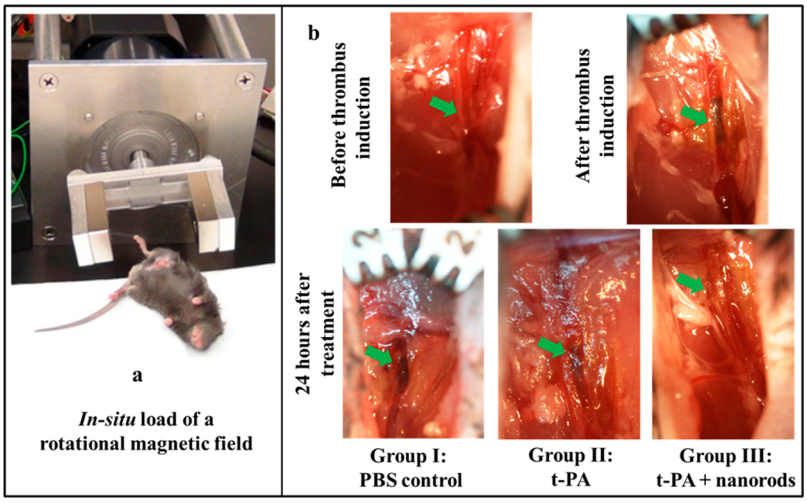

Figure 6. Enhanced thrombolysis by active nanomotors is demonstrated in a mice embolism model. (a) *In situ* experimental setup. (b) Thrombolysis evaluation in the right femoral vessels of mice belonging to three groups associated with different administrations. The green arrows indicate the inducted region in the femoral vessels of C57/BL6 mice.

C_R, the v_{R+T} can be significantly improved. This feature would reduce the potential side effects caused by nanorods for clinical application.[36]

To examine the proposed approach for thrombolytic treatment *in vivo*, we study femoral embolism in living mice by infusing t-PA dose with and without active nanomotors. For thrombosis induction, the femoral vessels of C57/BL6 mice (20−25 g) are damaged *via* solution of ferric chloride ($FeCl_3$) to the outer surface. This results in the formation of a thrombus within the vessel, the severity of which is controlled by the concentration of the $FeCl_3$ solution. At 10 min after the induction, retro-orbital intravenous t-PA (10 mg kg^{-1}) and nickel rod administration is started. Nickel rod solution (10 mg mL^{-1}) is previously prepared by sonicating in 1% poly(acrylic acid) solution and is injected into the mouse (100 mg kg^{-1}) together with or without t-PA. Then the infected hindlimb is put in the center of homemade rotating magnets (20 Hz) with magnetic field strength of 40 mT for 45 min, shown in Figure 6a. After 24 h, the mouse is anesthetized to check the previously formed thrombi in the femoral vessel. Mice are randomly divided into three groups. Group I (n = 2) is just treated intravenously with PBS as control. Group II (n = 4) is injected with t-PA solution. Group III (n = 3) is treated by combining t-PA with nickel rods. From the results shown in Figure 6b, the thrombus remains in all the mice of Group I while all the mice in Group II which receive t-PA injection have a little residual thrombus. However, in Group III, with both t-PA and Ni nanorods injected and treated in a rotating magnetic field, there are no residual thrombus left. This preliminary result demonstrates higher thrombus removal efficiency of the active nanomotor method.

CONCLUSION

We have developed a novel active nanomotor-based method to directly enhance t-PA-mediated thrombolysis. Compared with nanocarrier-based strategies that focus on the loading rate of specified drug molecules to specified nanocarriers, active motions of nanomotors accelerate the thrombolysis by elevating drug transport through a hydrodynamic convection, which is controlled by many parameters such as nanorod concentration, magnetic field, and frequency. The results illustrate that nanomotors can be used as an independent input to power the drug's efficacy and develop a safer and more effective medical treatment without immobilizing and encapsulating drug molecules. With further development, drug agitation by nanomotors could be an important step to treat clot in small blood vessels more specifically and safely and can also be used as a general principle for other disease treatment.

METHODS

Nanorod Fabrication and Preparation. The magnetic nanorods were fabricated by the OAD method.[25] OAD is a physical vapor deposition technique in which the substrate is normally positioned at a large angle with respect to deposition vapor direction. To fabricate uniform nickel nanorods on the substrate, a 500 nm diameter polystyrene bead monolayer was formed on a Si substrate using the convective self-assembly method.[37] The bead-coated substrates were loaded into a custom-built electron beam evaporation chamber. Nickel (99.95%, Alfa Aesar, Ward Hill, MA) was deposited at a vapor incident angle of 86° and at a rate of ~0.5 nm s^{-1}, monitored by a quartz crystal microbalance (QCM) facing directly toward the incident vapor. Ni nanorods of ~1 μm length were obtained when the QCM reading reached 2 μm, as shown in Figure 2a. To prevent the aggregation of the nanorods in solution, the Ni rods on substrates were dipped in PVP (MW = 360K Da, Sigma-Aldrich, St. Louis, MO) solution (w/w = 10%) for 24 h. Then the

substrates were sonicated for 1 min in another PVP (MW = 40K Da, Sigma-Aldrich, St. Louis, MO) solution (w/w = 10%) for 30 s. During the sonication, most of the rods were released from the substrates and suspended in PVP solution to form a stable matrix, as shown in Figure 2d. The final concentration of the nanorods was determined by the weight difference of substrates before and after the sonication. Before each experiment, the rods in the matrix were extracted by a strong permanent magnet, washed by water 2−3 times, and prepared to be mixed with reaction solutions.

Channel Fabrication and Preparation. Both *in vitro* clotting and thrombolysis were performed in channels fabricated by PDMS. The PDMS was mixed with the solidifying agent and poured in an aluminum mold after degassing in vacuum. Cured in an oven at 72 °C for 2 h, the PDMS plate was peeled off from the mold. Then, it was covalently bonded with another blanket flat PDMS plate to form the experimental plate with 8 comb-like 2×1 mm^2 rectangular channels (see Supporting Information 1.1). Two rows of 1 mm diameter holes were punched at 10 and 20 mm from the open ends. The first row of holes was used to inject the reaction solution, and the second row was used for the mineral oil to seal the reaction solution within the channels and prevent evaporation. To fabricate length-controlled clot in the PDMS channels, all the reagents and the channels were cooled in an ice box at 0 °C for 15 min. Then, 80 μL $\times$ 1 μM human thrombin (thrombin from human plasma, Sigma-Aldrich, St. Louis, MO) was added to 1 mL of HPPP (human platelet poor plasma, Innovative Research, Novi, MI), mixed by vortex. Since the enzyme catalytic reaction was slowed at the low temperature, the mixture remained as a flow-able "clot" in about 1 min. Within such a time scale, a 20 μL well-mixed thrombin and HPPP was injected from the end of each channel one by one to form a 10 mm long clot. Once the mixture was injected in the channels, it could not flow out due to the capillary force. Then the plate was immediately suspended in a pool of 4 mL of HPPP at 37 °C for 20 min. This allowed the residual agents in channels to continue reacting with HPPP sufficiently and reinforce the clot structures. After this process, the open ends of the device were sealed by epoxy and ready for the injection of reaction solution. The dye added to all the reaction solution was Rhodamine B (HPLC, Sigma-Aldrich, St. Louis, MO). The t-PA solution was liquefied from its lyophilized powder (Alteplase, Genentech, South San Francisco, CA).

***In Vitro* Experimental Data Treatment.** *In vitro* experimental data were obtained by a digital camera (Infinity 1, Lumenera Corp, Ottawa, Canada). ImageJ software (National Institutes of Health, Bethesda, MD) was used to decompose images into red, green, and blue channels. The boundaries of the liquid/clot were identified based on the grayscale value of images in the green channel since Rhodamine B absorbs most of the green light and maximizes the contrast. The grayscale plot shown in Figure 3c was obtained by averaging the grayscale value vertically across the PDMS channel and was then converted to the concentration of dye molecules according to Beer's law. A calibration curve was produced using known concentrations of dye solution in PDMS channels (see Supporting Information 1.2). The boundary position of the liquid/clot was defined as the maximum gradient of concentration in the *x*-direction and was collected from different channels at different time points. Lastly, Matlab (The MathWorks, Natick, MA) was used to fit the boundary moving speed of each channel.

***In Vivo* Experiment Setup.** To induce thrombosis, C57/BL6 mice (20−25 g) were initially anesthetized using intraperitoneal ketamine (60 mg kg^{-1}) and xylazine (10 mg kg^{-1}). After exposure, on the right femoral vessel, $FeCl_3$ was topically applied to the femoral vein using a 1×1 mm^2 strip of filter paper soaked in 20% $FeCl_3$ solution. The filter paper was applied to the anterior surface of the vein for 5 min. Then, the strip was removed, and the vessel was washed with PBS. After $FeCl_3$ induction, mice femoral vein formed the visible thrombus, shown in Figure 6b. The magnetic field used to active nanomotors inside the mice bodies was produced by a pair of permanent magnets (NdFeB, BY0X08DCS, K&J, Pipersville, PA) with their poles attractively facing each other. The magnets were fixed on an aluminous rotator which was connected to a speed control AC motor (US560-001U2, Oriental Motor, Torrance, CA), shown in Figure 6a. To meet the experimental requirements, the field strength was adjusted by the distance between the magnets (see Supporting Information 1.3), and the field frequency was controlled by the rotational speed of the AC motor.

Conflict of Interest: The authors declare no competing financial interest.

Acknowledgment. This work is supported by National Science Foundation under contracts ECCS-09011, ECCS-1303134, and ECCS-1150042, and National Institutes of Health under contract R21 NS084148-01A1.

Supporting Information Available: In vitro and *in vivo* experimental setup, theoretical derivation on thrombolytic enhancement, and videos of *in vitro* thrombolysis in PDMS channels are included. This material is available free of charge *via* the Internet at http://pubs.acs.org.

REFERENCES AND NOTES

1. Laverdure, A. M.; Surbeck, J.; North, M. O.; Tritto, J. Growth, Development, Reproduction, Physiological and Behavioural Studies on Living Organisms, Human Adults and Children Exposed to Radiation from Video Displays. *Indoor Built Environ.* **2001**, *10*, 306–309.
2. Alexandrov, A. V.; Molina, C. A.; Grotta, J. C.; Garami, Z.; Ford, S. R.; Alvarez-Sabin, J.; Montaner, J.; Saqqur, M.; Demchuk, A. M.; Moye, L. A.; *et al.* Ultrasound-Enhanced Systemic Thrombolysis for Acute Ischemic Stroke. *N. Engl. J. Med.* **2004**, *351*, 2170–2178.
3. Mohr, J. P. Thrombolytic Therapy for Ischemic Stroke: From Clinical Trials to Clinical Practice. *JAMA* **2000**, *283*, 1189–1191.
4. Adams, H. P., Jr.; del Zoppo, G.; Alberts, M. J.; Bhatt, D. L.; Brass, L.; Furlan, A.; Grubb, R. L.; Higashida, R. T.; Jauch, E. C.; Kidwell, C.; *et al.* Guidelines for the Early Management of Adults with Ischemic Stroke: A Guideline from the American Heart Association/American Stroke Association Stroke Council, Clinical Cardiology Council, Cardiovascular Radiology and Intervention Council, and the Atherosclerotic Peripheral Vascular Disease and Quality of Care Outcomes in Research Interdisciplinary Working Groups: The American Academy of Neurology Affirms the Value of This Guideline as an Educational Tool for Neurologists. *Stroke* **2007**, *38*, 1655–1711.
5. Rosengart, A. J.; Kaminski, M. D.; Ghebremeskel, A.; Johns, L.; Kaza, K.; Novakovic, R.; Wardrip, C.; Frank, J. I.; Macdonald, R. L. Advancing toward Magnetically Guided, Targeted Delivery of Tissue Plasminogen Activator: Preliminary Flow Studies in the Primate Model. *Stroke* **2004**, *35*, 299.
6. Abdalla, A.; Mader, K. ESR Studies on the Influence of Physiological Dissolution and Digestion Media on the Lipid Phase Characteristics of Sedds and Sedds Pellets. *Int. J. Pharm.* **2009**, *367*, 29–36.
7. Kaminski, M. D.; Xie, Y.; Mertz, C. J.; Finck, M. R.; Chen, H.; Rosengart, A. J. Encapsulation and Release of Plasminogen Activator from Biodegradable Magnetic Microcarriers. *Eur. J. Pharm. Sci.* **2008**, *35*, 96–103.
8. Chen, A. P.; Bi, Z. X.; Tsai, C. F.; Chen, L.; Su, Q.; Zhang, X. H.; Wang, H. Y. Tilted Aligned Epitaxial $La_{0.7}Sr_{0.3}MnO_3$ Nanocolumnar Films with Enhanced Low-Field Magnetoresistance by Pulsed Laser Oblique-Angle Deposition. *Cryst. Growth Des.* **2011**, *11*, 5405–5409.
9. Myerson, J.; He, L.; Lanza, G.; Tollefsen, D.; Wickline, S. Thrombin-Inhibiting Perfluorocarbon Nanoparticles Provide a Novel Strategy for the Treatment and Magnetic Resonance Imaging of Acute Thrombosis. *J. Thromb. Haemostasis* **2011**, *9*, 1292–1300.
10. Korin, N.; Kanapathipillai, M.; Matthews, B. D.; Crescente, M.; Brill, A.; Mammoto, T.; Ghosh, K.; Jurek, S.; Bencherif, S. A.; Bhatta, D.; *et al.* Shear-Activated Nanotherapeutics for Drug Targeting to Obstructed Blood Vessels. *Science* **2012**, *337*, 738–742.
11. Marsh, J. N.; Senpan, A.; Hu, G.; Scott, M. J.; Gaffney, P. J.; Wickline, S. A.; Lanza, G. M. Fibrin-Targeted Perfluorocarbon

Nanoparticles for Targeted Thrombolysis. *Nanomedicine* **2007**, *2*, 533–543.
12. Adams, H. P.; del Zoppo, G.; Alberts, M. J.; Bhatt, D. L.; Brass, L.; Furlan, A.; Grubb, R. L.; Higashida, R. T.; Jauch, E. C.; Kidwell, C.; *et al.* Guidelines for the Early Management of Adults with Ischemic Stroke—A Guideline from the American Heart Association/American Stroke Association Stroke Council, Clinical Cardiology Council, Cardiovascular Radiology and Intervention Council, and the Atherosclerotic Peripheral Vascular Disease and Quality of Care Outcomes in Research Interdisciplinary Working Groups (Reprinted from Stroke, Vol 38, Pg 1655−1711, 2007). *Circulation* **2007**, *115*, E478–E534.
13. del Zoppo, G. J.; Saver, J. L.; Jauch, E. C.; Adams, H. P., Jr. American Heart Association Stroke, C. Expansion of the Time Window for Treatment of Acute Ischemic Stroke with Intravenous Tissue Plasminogen Activator: A Science Advisory from the American Heart Association/American Stroke Association. *Stroke* **2009**, *40*, 2945–2948.
14. Feldschuh, J.; Enson, Y. Prediction of the Normal Blood Volume. Relation of Blood Volume to Body Habitus. *Circulation* **1977**, *56*, 605–612.
15. Seifried, E.; Tanswell, P.; Ellbruck, D.; Haerer, W.; Schmidt, A. Pharmacokinetics and Haemostatic Status during Consecutive Infusions of Recombinant Tissue-Type Plasminogen Activator in Patients with Acute Myocardial Infarction. *Thromb. Haemostasis* **1989**, *61*, 497–501.
16. Tanswell, P.; Seifried, E.; Stang, E.; Krause, J. Pharmacokinetics and Hepatic Catabolism of Tissue-Type Plasminogen Activator. *Arzneimittelforschung* **1991**, *41*, 1310–1319.
17. Yeo, L. L.; Paliwal, P.; Teoh, H. L.; Seet, R. C.; Chan, B. P.; Liang, S.; Venketasubramanian, N.; Rathakrishnan, R.; Ahmad, A.; Ng, K. W.; *et al.* Timing of Recanalization after Intravenous Thrombolysis and Functional Outcomes after Acute Ischemic Stroke. *JAMA Neurol.* **2013**, *70*, 353–358.
18. Riedel, C. H.; Zimmermann, P.; Jensen-Kondering, U.; Stingele, R.; Deuschl, G.; Jansen, O. The Importance of Size: Successful Recanalization by Intravenous Thrombolysis in Acute Anterior Stroke Depends on Thrombus Length. *Stroke* **2011**, *42*, 1775–1777.
19. Wu, J. H.; Siddiqui, K.; Diamond, S. L. Transport Phenomena and Clot Dissolving Therapy: An Experimental Investigation of Diffusion-Controlled and Permeation-Enhanced Fibrinolysis. *Thromb. Haemostasis* **1994**, *72*, 105–112.
20. Diamond, S. L.; Anand, S. Inner Clot Diffusion and Permeation During Fibrinolysis. *Biophys. J.* **1993**, *65*, 2622–2643.
21. Anand, S.; Wu, J. H.; Diamond, S. L. Enzyme-Mediated Proteolysis of Fibrous Biopolymers: Dissolution Front Movement in Fibrin or Collagen under Conditions of Diffusive or Convective Transport. *Biotechnol. Bioeng.* **1995**, *48*, 89–107.
22. Garber, P. J.; Mathieson, A. L.; Ducas, J.; Patton, J. N.; Geddes, J. S.; Prewitt, R. M. Thrombolytic Therapy in Cardiogenic Shock: Effect of Increased Aortic Pressure and Rapid Tpa Administration. *Can. J. Cardiol.* **1995**, *11*, 30–36.
23. Prewitt, R. M.; Gu, S.; Garber, P. J.; Ducas, J. Marked Systemic Hypotension Depresses Coronary Thrombolysis Induced by Intracoronary Administration of Recombinant Tissue-Type Plasminogen Activator. *J. Am. Coll. Cardiol.* **1992**, *20*, 1626–1633.
24. Kumbasar, S. D.; Semiz, E.; Ermis, C.; Yalcinkaya, S.; Deger, N.; Pamir, G.; Oral, D. Effect of Intraaortic Balloon Counter-Pulsation on Qt Dispersion in Acute Anterior Myocardial Infarction. *Int. J. Cardiol.* **1998**, *65*, 169–172.
25. He, Y.; Fu, J.; Zhang, Y.; Zhao, Y.; Zhang, L.; Xia, A.; Cai, J. Multilayered Si/Ni Nanosprings and Their Magnetic Properties. *Small* **2007**, *3*, 153–160.
26. Kaplan, A. P.; Castellino, F. J.; Collen, D.; Wiman, B.; Taylor, F. B., Jr. Molecular Mechanisms of Fibrinolysis in Man. *Thromb. Haemostasis* **1978**, *39*, 263–283.
27. Collen, D. Molecular Mechanisms of Fibrinolysis and Their Application to Fibrin-Specific Thrombolytic Therapy. *J. Cell. Biochem.* **1987**, *33*, 77–86.
28. Collen, D. Molecular Mechanisms of Fibrinolysis and Thrombolysis. *Therapie* **1988**, *43*, 69.
29. Cesarman-Maus, G.; Hajjar, K. A. Molecular Mechanisms of Fibrinolysis. *Br. J. Hamaetol.* **2005**, *129*, 307–321.
30. Collen, D.; Lijnen, H. R. The Tissue-Type Plasminogen Activator Story. *Arterioscler., Thromb., Vasc. Biol.* **2009**, *29*, 1151–1155.
31. Calef, D. F.; Deutch, J. M. Diffusion-Controlled Reactions. *Annu. Rev. Phys. Chem.* **1983**, *34*, 493–524.
32. McCarty, P.; Horsthemke, W. Effective Diffusion Coefficient for Steady Two-Dimensional Convective Flow. *Phys. Rev. A* **1988**, *37*, 2112–2117.
33. Rosenbluth, M. N.; Berk, H. L.; Doxas, I.; Horton, W. Effective Diffusion in Laminar Convective Flows. *Phys. Fluids* **1987**, *30*, 2636–2647.
34. Sagues, F.; Horsthemke, W. Diffusive Transport in Spatially Periodic Hydrodynamic Flows. *Phys. Rev. A* **1986**, *34*, 4136–4143.
35. Petousis, I.; Homburg, E.; Derks, R.; Dietzel, A. Transient Behaviour of Magnetic Micro-Bead Chains Rotating in a Fluid by External Fields. *Lab Chip* **2007**, *7*, 1746–1751.
36. Radomski, A.; Jurasz, P.; Alonso-Escolano, D.; Drews, M.; Morandi, M.; Malinski, T.; Radomski, M. W. Nanoparticle-Induced Platelet Aggregation and Vascular Thrombosis. *Br. J. Pharmacol.* **2005**, *146*, 882–893.
37. Zhao, Y. P.; Ye, D. X.; Wang, G. C.; Lu, T. M. Novel Nano-Column and Nano-Flower Arrays by Glancing Angle Deposition. *Nano Lett.* **2002**, *2*, 351–354.